Surface-enhanced terahertz spectroscopy using gold rod structures resonant with terahertz waves

Kosei Ueno,[1,*] Sho Nozawa,[1] and Hiroaki Misawa[1,2]

[1]*Research Institute for Electronic Science, Hokkaido University, N21, W10, Kita-ku, 001-0021, Sapporo, Japan*
[2]*Department of Applied Chemistry & Institute of Molecular Science, National Chiao Tung University, 1001 Ta Hsueh R., Hsinchu 30010, Taiwan*
[*]*k-ueno@es.hokudai.ac.jp*

Abstract: Terahertz (THz) spectroscopy is a promising method to measure the spectrum of low-frequency modes of molecules or ensembles, such as crystals and polymers, including proteins. However, the main drawback of THz spectroscopy is its extremely low sensitivity. In the present study, we report on signal enhancement in THz spectroscopy achieved by depositing amino acid molecules or their derivatives on a gold rod structured silicon substrate whose localized surface plasmon resonance is exhibited in the THz frequency region. The distinct peaks derived from the enhancement of the inherent spectrum based on a molecular crystal were clearly observed when a longitudinal plasmon resonance mode of the gold rod structure was excited and the plasmon resonance band overlapped the molecular/intermolecular vibrational mode. We discuss the mechanism by which surface-enhanced THz spectroscopy was induced from the viewpoint of the enhancement of light-matter coupling due to plasmon excitation and the modulation of the plasmon band by dipole coupling between the plasmon dipole and molecular/intermolecular vibrational modes.

OCIS codes: (240.6680) Surface plasmons; (300.6490) Spectroscopy, surface.

References and links

1. S. Link and M. A. El-Sayed, "Spectral properties and relaxation dynamics of surface plasmon electronic oscillations in gold and silver nanodots and nanorods," J. Phys. Chem. B **103**(40), 8410–8426 (1999).
2. K. A. Willets and R. P. Van Duyne, "Localized surface plasmon resonance spectroscopy and sensing," Annu. Rev. Phys. Chem. **58**(1), 267–297 (2007).
3. H. Xu, J. Aizpurua, M. Käll, and P. Apell, "Electromagnetic contributions to single-molecule sensitivity in surface-enhanced raman scattering," Phys. Rev. E Stat. Phys. Plasmas Fluids Relat. Interdiscip. Topics **62**(3), 4318–4324 (2000).
4. K. L. Kelly, E. Coronado, L. L. Zhao, and G. C. Schatz, "The optical properties of metal nanoparticles: the influence of size, shape, and dielectric environment," J. Phys. Chem. B **107**(3), 668–677 (2003).
5. S. Nie and S. R. Emory, "Probing single molecules and single nanoparticles by surface-enhanced Raman scattering," Science **275**(5303), 1102–1106 (1997).
6. K. Kneipp, Y. Wang, H. Kneipp, L. T. Perelman, I. Itzkan, R. R. Dasari, and M. S. Feld, "Single molecule detection using surface-enhanced Raman scattering (SERS)," Phys. Rev. Lett. **78**(9), 1667–1670 (1997).
7. J. R. Lakowicz, Y. Shen, S. D'Auria, J. Malicka, J. Fang, Z. Gryczynski, and I. Gryczynski, "Radiative decay engineering. 2. Effects of Silver Island films on fluorescence intensity, lifetimes, and resonance energy transfer," Anal. Biochem. **301**(2), 261–277 (2002).
8. S. Gao, K. Ueno, and H. Misawa, "Plasmonic antenna effects on photochemical reactions," Acc. Chem. Res. **44**(4), 251–260 (2011).
9. M. S. Tame, K. R. McEnery, S. K. Ozdemir, J. Lee, S. A. Maier, and M. S. Kim, "Quantum plasmonics," Nat. Phys. **9**(6), 329–340 (2013).
10. K. Liu, M. G. Brown, and R. J. Saykally, "Terahertz laser vibration rotation tunneling spectroscopy and dipole moment of a cage form of the water hexamer," J. Phys. Chem. A **101**(48), 8995–9010 (1997).
11. A. G. Markelz, A. Roitberg, and E. J. Heilweil, "Pulsed terahertz spectroscopy of DNA, bovine serum albumin and collagen between 0.1 and 2.0 THz," Chem. Phys. Lett. **320**(1-2), 42–48 (2000).
12. K. L. Nguyen, T. Friscić, G. M. Day, L. F. Gladden, and W. Jones, "Terahertz time-domain spectroscopy and the quantitative monitoring of mechanochemical cocrystal formation," Nat. Mater. **6**(3), 206–209 (2007).

#249242 Received 1 Sep 2015; revised 17 Oct 2015; accepted 21 Oct 2015; published 23 Oct 2015

13. T. Globus, D. Woolard, T. W. Crowe, T. Khromova, B. Gelmont, and J. Hesler, "Terahertz Fourier transform characterization of biological materials in a liquid phase," J. Phys. D Appl. Phys. **39**(15), 3405–3413 (2006).
14. R. Balu, H. Zhang, E. Zukowski, J. Y. Chen, A. G. Markelz, and S. K. Gregurick, "Terahertz spectroscopy of bacteriorhodopsin and rhodopsin: similarities and differences," Biophys. J. **94**(8), 3217–3226 (2008).
15. E. Goormaghtigh, V. Cabiaux, and J. M. Ruysschaert, "Secondary structure and dosage of soluble and membrane proteins by attenuated total reflection Fourier-transform infrared spectroscopy on hydrated films," Eur. J. Biochem. **193**(2), 409–420 (1990).
16. T. Arikawa, M. Nagai, and K. Tanaka, "Characterizing hydration state in solution using terahertz time-domain attenuated total reflection spectroscopy," Chem. Phys. Lett. **457**(1-3), 12–17 (2008).
17. C. Debus and P. H. Bolivar, "Frequency selective surfaces for high sensitivity terahertz sensing," Appl. Phys. Lett. **91**(18), 184102 (2007).
18. Z. Tian, J. Han, X. Lu, J. Gu, Q. Xing, and W. Zhang, "Surface plasmon enhanced terahertz spectroscopic distinguishing between isotopes," Chem. Phys. Lett. **475**(1-3), 132–134 (2009).
19. G. Ramakrishnan, N. Kumar, P. C. M. Planken, D. Tanaka, and K. Kajikawa, "Surface plasmon-enhanced terahertz emission from a hemicyanine self-assembled monolayer," Opt. Express **20**(4), 4067–4073 (2012).
20. C. Feuillet-Palma, Y. Todorov, A. Vasanelli, and C. Sirtori, "Strong near field enhancement in THz nano-antenna arrays," Sci. Rep. **3**, 1361 (2013).
21. Y.-M. Bahk, G. Ramakrishnan, J. Choi, H. Song, G. Choi, Y. H. Kim, K. J. Ahn, D.-S. Kim, and P. C. M. Planken, "Plasmon enhanced terahertz emission from single layer graphene," ACS Nano **8**(9), 9089–9096 (2014).
22. S. Bagiante, F. Enderli, J. Fabiańska, H. Sigg, and T. Feurer, "Giant electric field enhancement in split ring resonators featuring nanometer-sized gaps," Sci. Rep. **5**, 8051 (2015).
23. L. Xie, W. Gao, J. Shu, Y. Ying, and J. Kono, "Extraordinary sensitivity enhancement by metasurfaces in terahertz detection of antibiotics," Sci. Rep. **5**, 8671 (2015).
24. Z. Han, Y. Zhang, and S. I. Bozhevolnyi, "Spoof surface plasmon-based stripe antennas with extreme field enhancement in the terahertz regime," Opt. Lett. **40**(11), 2533–2536 (2015).
25. K. Ueno, V. Mizeikis, S. Juodkazis, K. Sasaki, and H. Misawa, "Optical properties of nanoengineered gold blocks," Opt. Lett. **30**(16), 2158–2160 (2005).
26. K. Ueno and H. Misawa, "Spectral properties and electromagnetic field enhancement effects on nano-engineered metallic nanoparticles," Phys. Chem. Chem. Phys. **15**(12), 4093–4099 (2013).
27. L. Razzari, A. Toma, M. Shalaby, M. Clerici, R. P. Zaccaria, C. Liberale, S. Marras, I. A. I. Al-Naib, G. Das, F. De Angelis, M. Peccianti, A. Falqui, T. Ozaki, R. Morandotti, and E. Di Fabrizio, "Extremely large extinction efficiency and field enhancement in terahertz resonant dipole nanoantennas," Opt. Express **19**(27), 26088–26094 (2011).
28. H. Yasuda and I. Hosako, "Measurement of terahertz refractive index of metal with terahertz time-domain spectroscopy," Jpn. J. Appl. Phys. **47**(3), 1632–1634 (2008).
29. A. Shalabney, J. George, J. Hutchison, G. Pupillo, C. Genet, and T. W. Ebbesen, "Coherent coupling of molecular resonators with a microcavity mode," Nat. Commun. **6**, 5981 (2015).
30. J. George, A. Shalabney, J. A. Hutchison, C. Genet, and T. W. Ebbesen, "Liquid-phase vibrational strong coupling," J. Phys. Chem. Lett. **6**(6), 1027–1031 (2015).
31. J. Bellessa, C. Bonnand, J. C. Plenet, and J. Mugnier, "Strong coupling between surface plasmons and excitons in an organic semiconductor," Phys. Rev. Lett. **93**(3), 036404 (2004).
32. Y. Sugawara, T. A. Kelf, J. J. Baumberg, M. E. Abdelsalam, and P. N. Bartlett, "Strong coupling between localized plasmons and organic excitons in metal nanovoids," Phys. Rev. Lett. **97**(26), 266808 (2006).
33. N. T. Fofang, T.-H. Park, O. Neumann, N. A. Mirin, P. Nordlander, and N. J. Halas, "Plexcitonic nanoparticles: plasmon-exciton coupling in nanoshell-J-aggregate complexes," Nano Lett. **8**(10), 3481–3487 (2008).
34. T. Itoh, Y. S. Yamamoto, H. Tamaru, V. Biju, S.-i. Wakida, and Y. Ozaki, "Single-molecular surface-enhanced resonance Raman scattering as a quantitative probe of local electromagnetic field: The case of strong coupling between plasmonic and excitonic resonance," Phys. Rev. B **89**(19), 195436 (2014).
35. I. Sugimoto, S. Maeda, Y. Suda, K. Makihara, and K. Takahashi, "Low-vacuum deposition of glutamic acid and pyroglutamic acid: a facile methodology for depositing organic materials beyond amino acids," J. Amino Acids **2014**, 434056 (2014).
36. H. Wu, N. Reeves-McLaren, S. Jones, R. I. Ristic, J. P. A. Fairclough, and A. R. West, "Phase transformations of glutamic acid and its decomposition products," Cryst. Growth Des. **10**(2), 988–994 (2010).
37. N. Yamamoto, O. Kambara, K. Yamamoto, A. Tamura, S. Saito, and K. Tominaga, "Temperature and hydration dependence of low-frequency spectra of poly-l-glutamic acid with different secondary structures studied by terahertz time-domain spectroscopy," Soft Matter **8**(6), 1997–2006 (2012).

1. Introduction

Nanoparticles of metals, such as gold and silver, exhibit very intense colors derived from localized surface plasmon resonance (LSPR) [1,2]. Plasmon resonances, which are collective oscillations of conduction electrons, promote the enhancement of the electromagnetic field in the vicinity of metallic nanoparticles [3,4]. Various optical effects, such as surface-enhanced Raman scattering and fluorescence enhancement, are promoted by LSPR excitation [5–7]. One reason why such optical effects are promoted by LSPR is that the light-matter coupling

#249242 Received 1 Sep 2015; revised 17 Oct 2015; accepted 21 Oct 2015; published 23 Oct 2015

efficiency is enhanced by the electromagnetic field enhancement effect [8,9]. In particular, surface-enhanced spectroscopies are a powerful means to analyze a small number of molecules for a chemical sensor application.

Terahertz (THz) spectroscopy has received considerable attention because the energy of a THz wave is close to that of intermolecular interactions, such as hydrogen bonding, van der Waals force, the lattice vibration of a crystal, and the translational and rotational energy of a molecule [10–12]. The advantage of THz spectroscopy is that it can measure the spectrum of low-frequency modes of a molecule even with a light element or in an ensemble, such as a crystal or polymer [13,14]. Therefore, THz spectroscopy is occasionally used complementarily with neutron scattering. However, one of the drawbacks of THz spectroscopy is its extremely low sensitivity due to the low probability of interaction between the THz wave and the molecular/intermolecular vibrational modes.

Regarding near-infrared spectroscopy, a small number of molecules deposited on a substrate can be measured using attenuated total reflection (ATR) methods because the apparent optical path length increases, allowing the probe light to perform multiple reflections through the sample under the total-internal-reflection conditions [15]. Of course, this concept can also be applied to THz spectroscopy [16]. However, in the case of THz spectroscopy, the probe light might be attenuated by adsorbed water molecules or contained to the sample due to strong absorption in the THz frequency region. That is, lengthening of the optical path length is not suitable for the enhancement of THz spectroscopy, and thus light confinement for a relatively longer time is necessary due to the slow group velocity of the THz wave for the enhancement of light-matter coupling efficiency.

Recently, various micro- and nanostructures, such as a metallic hole array, a ring resonator as well as a spoof surface plasmon based antenna using metal stripes, which are coupled with the THz wave and exhibit near-field enhancement effects, have been reported [17–24]. In the present study, we aim to elucidate surface-enhanced THz spectroscopy using a simple gold rod structure. The gold rod structure is promising because it is easy to tune the plasmon resonant wavelength from visible to infrared wavelength by changing the aspect ratio of the gold rod structures. These structures exhibit strong enhancement of the electromagnetic field similarly to a metallic hole array or a ring resonator. The control of linear polarized light can allow for selective excitation of LSPR under the incident polarization parallel and perpendicular to the gold rod structure [25]. That is, only the longitudinal plasmon resonance band is in the THz frequency. Therefore, a systematic study can be performed to understand whether the signal enhancement of THz spectroscopy is induced by the effect of LSPR excitation by measuring the LSPR band compared with a molecular/intermolecular vibrational mode and pursuing an incident polarization effect.

In this study, we successfully demonstrate surface-enhanced THz spectroscopy of an amino acid molecule and its derivatives deposited on gold rod structures fabricated on a silicon substrate. The spectral properties of the gold rod structures in the THz frequency region were studied. We discussed the mechanism by which surface-enhanced THz spectroscopy was induced from the viewpoint of the enhancement of light-matter coupling due to LSPR excitation and modulation by dipole coupling between the plasmon dipole and molecular/intermolecular vibrational modes.

2. Experimental

Gold rod structures were fabricated on silicon substrates using electron beam lithography and lift-off techniques [26]. After washing a silicon substrate with acetone, methanol, and pure water, the positive resist film for electron beam lithography (ZEP520a, Zeon Chemicals Co.) was formed via spin-coating to a thickness of 200 nm on the substrate. The spin-coated film was exposed to a given pattern using an electron beam lithography system (ELS-7000, Elionix Co.) with an accelerating voltage of 100 kV. The area patterned by electron beam exposure was 5 mm × 5 mm. The exposed resist film was then developed and rinsed using a developer solution (Anisole, Wako Pure Chemical Industries, Ltd.) and a rinsing agent (ZMD-B, Zeon Chemicals Co.). A thin film of gold was then deposited via sputtering onto the

#249242 Received 1 Sep 2015; revised 17 Oct 2015; accepted 21 Oct 2015; published 23 Oct 2015

developed substrate (MPS-4000C1/HC1, ULVAC Co.), and the resist layer below the gold film was removed with a resist remover solution (ZDMAC, Zeon Chemicals Co.), resulting in the formation of gold nanorod structures on the substrate.

A conventional THz time-domain spectroscopy system was constructed for the measurement of the extinction spectrum in the THz frequency region from 0.1 to 1 THz. A femtosecond laser pulse with a center wavelength of 800 nm (τ_p: 25 fs, f: 80 MHz, Griffin, KM Labs, Inc.) was split into two laser pulses using a beam splitter and focused onto the photoconductive antennae (PCA-44-06-10-800, Batop optoelectronics Gmbh) via an optical delay scanner for the probe pulse (OROCHI F-Pack660/680, Photo-Physcis Co.) to measure the THz time-domain signal. The extinction spectrum was obtained by recording two spectra of the light transmitted through the sample and through a substrate as a reference. For the measurement of the extinction spectrum of the gold rod structures in the frequency region from 1 to 3 THz, a THz time-domain spectroscopy system (TAS7400, Advantest Co.) was employed. The extinction spectrum in the near-infrared wavelength region was measured by a Fourier-transform infrared (FT-IR) spectrometer equipped with a microscope attachment (FT-IR, IRT-3000, Jasco Co.)

3. Results and discussion

3.1 Spectral properties of gold rods

A typical scanning electron microscope (SEM) image of a gold rod structure is presented in Fig. 1(a). Ordered arrays of gold rod structures 200 nm wide, 100 μm long and 40 nm thick were clearly observed on the silicon substrate. The distance between each structure from edge to edge was set at 10 μm in both the longitudinal and transverse directions. In this study, the width and thickness of a gold rod structure were set at identical values, and only the length was controlled to tune the LSPR peak frequency. Extinction spectra of the gold rod structures with different rod lengths are presented in Fig. 1(b). The incident linear polarization was set parallel to the gold rod structure. LSPR bands in the longitudinal mode were clearly observed as similar to the spectrum property of terahertz resonant dipole nanoantennas using gold [27], and the peak frequency exhibited a spectrum shift to a lower frequency region with increasing rod length. Importantly, not only the dipole resonance mode but also higher-order plasmon resonance modes were observed. This observation was especially prevalent in the gold rod structure with a lower aspect ratio, which was judged from the asymmetrical spectrum shape. Therefore, it is expected that the electromagnetic field enhancement effect is obtained with a relatively wide spectrum range.

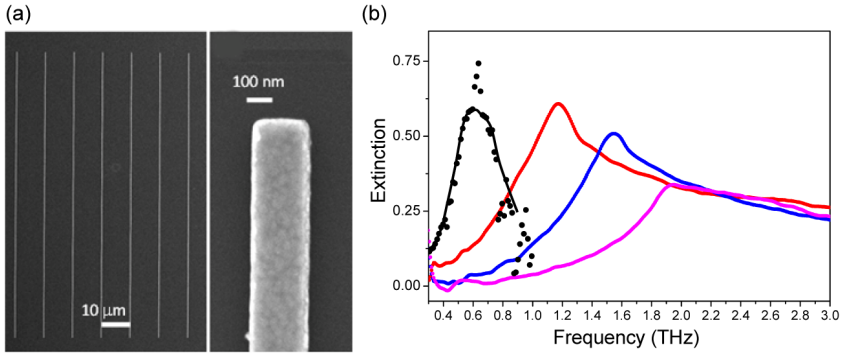

Fig. 1. (a) SEM image of gold rod structures 200 nm wide, 100 μm long and 40 nm thick. (b) Extinction spectra of gold rod structures with different rod lengths. Black: 100 μm, red: 50 μm, blue: 35 μm, and pink: 25 μm.

Figure 2(a) depicts a rod length dependence of the LSPR peak wavelength in the longitudinal mode. A linear relationship between the rod length and LSPR peak wavelength was obtained. As a separate experiment, gold nanorods that were 40 nm wide, of arbitrary

#249242 Received 1 Sep 2015; revised 17 Oct 2015; accepted 21 Oct 2015; published 23 Oct 2015

length, and 40 thick were fabricated, and their spectral properties were elucidated for comparison in the THz frequency region and near-infrared wavelength region. Figure 2(b) depicts the nanorod length dependence of the LSPR peak wavelength, and the inset highlights extinction spectra in the longitudinal mode with a different nanorod length. Analogous to the spectrum of the gold rod structures, the asymmetrical shape of the LSPR bands due to the higher-order plasmon resonance modes was clearly observed, and a spectral shift to a lower frequency region was confirmed with increasing nanorod length. Moreover, the linear relationship between the nanorod length and the LSPR peak wavelength was also clearly observed. Therefore, it was concluded that the spectral properties of the gold rods in the THz frequency region are very similar to the LSPR properties of gold nanorods in the near-infrared wavelength region. Finite-difference time-domain (FDTD, Lumerical Solutions, Inc.) simulation was performed using a gold rod design that was 200 nm wide, 80 μm long, and 40 nm thick. The dielectric constant of gold was taken from a literature [28]. The electromagnetic field enhancement effect with an enhancement factor ($|E|^2$) as great as 28000 was estimated at the plasmon resonant frequency (0.6 THz) around the four corners of the gold rod structure. Therefore, strong enhancement of the electromagnetic field is induced in the vicinity of the gold rod structures in the THz frequency region. From the spectral width presented in Fig. 1(b), the dephasing time (T_2, phase relaxation time) of the LSPR was estimated to be 0.8 ps for a gold rod structure 100 μm in length. Such a long dephasing time was obtained due to the relatively lower resonant frequency. Therefore, strong enhancement of the electromagnetic field was induced.

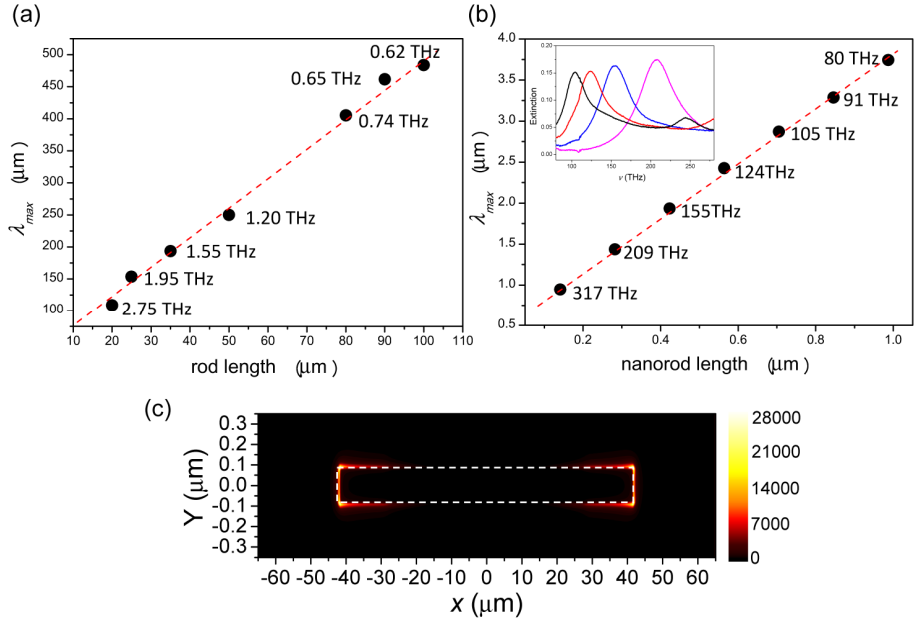

Fig. 2. (a) Rod length dependence of the LSPR peak wavelength. The inset numeric depicts the resonant frequency. (b) Nanorod length dependence of the LSPR peak wavelength. The inset figure and number indicate the extinction spectra of the gold nanorods and the resonant frequency for features of various lengths. Black: 700 nm, red: 560 nm, blue: 420 nm, and pink: 280 nm. (c) Near-field intensity distribution of a gold rod design that was 200 nm wide, 80 μm long, and 40 nm thick at the plasmon resonant frequency.

3.2 Surface-enhanced THz spectroscopy

The extinction spectrum of L-sodium glutamate pellet with a thickness of 0.9 mm is presented in Fig. 3(a). A characteristic band at approximately 22 to 23 cm^{-1} (0.66-0.69 THz) was clearly observed. Most importantly, strong peaks at approximately 24 cm^{-1} (0.72 THz) were

#249242 Received 1 Sep 2015; revised 17 Oct 2015; accepted 21 Oct 2015; published 23 Oct 2015

obviously observed overlapping with the LSPR band as noted in Fig. 3(b) after the L-sodium glutamate aqueous solution (20 mM) was drop cast onto the gold rod (length: 100 μm) structured silicon substrate and air-dried. In this experiment, the spectrum measured under the incident polarization perpendicular to the gold rod structure (transverse mode) was used as a reference for the extinction spectrum measurement. Therefore, the peaks observed in Fig. 3(b) are exclusively derived from the enhancement of the inherent spectrum based on the sodium glutamate crystal. Furthermore, such a peak could not be observed when the solution was only dropped on the silicon substrate without the gold rod structures. That is, the phenomenon was exclusively observed under the conditions at which the longitudinal plasmon resonance mode was excited. In Fig. 3(b), the frequency ranging from 16 to 19 cm^{-1} also extraordinarily enhanced the signals. That is, the LSPR band is divided into two peaks at shorter and longer wavelengths compared with the original LSPR band after the deposition of L-sodium glutamate. It is possible that the apparent absorption cross-section was enhanced due to the longer dephasing time of the LSPR. In addition, the plasmon resonant spectrum was modulated by the change of the dielectric function by the coupling between the plasmon dipole and the dipole moment of the molecular/intermolecular vibrational modes. Recently, Ebbesen et al. reported strong coupling between a microcavity and molecular vibrational modes, such as a C = O stretching vibrational mode in the near-infrared wavelength region and Rabi splitting in the spectrum [29,30]. We hypothesize that a similar dipole coupling between the molecular/intermolecular vibrational mode and the plasmon mode is induced even in the THz frequency region given that the shape of the LSPR band also changed after the deposition of L-sodium glutamate molecules and split into two peaks ranging over the LSPR band, as presented in Fig. 3(b). Therefore, this phenomenon is similar to the strong coupling or Fano resonance. If this is a strong coupling regime, the Rabi splitting energy can be roughly estimated to be about 0.6 meV although a dispersion curve measurement is necessary to obtain the precise Rabi splitting energy. It is known that the Rabi splitting energy of plasmon-exciton strong coupling system is around several 100 meV in visible wavelength region [31–34]. On the other hand, in near-infrared wavelength region, the vacuum Rabi splitting energy between microcavity and C = O stretching vibrational mode was reported as about 20 meV [29]. Namely, the Rabi splitting energy is qualitatively lower than 1/10 ~1/4 of the plasmon resonant energy or the energy of microcavity mode. In this study, the plasmon resonant energy in THz frequency region is about 2.5 meV. Although the Rabi splitting energy estimated as 0.6 meV seems to be very low value, the Rabi splitting energy is by no means small in THz frequency region. On the other hand, the LSPR band exhibited a spectral shift slightly to the lower frequency region after the deposition of the molecules (Fig. 3(b)) because the refractive index of the surrounding medium changed due to the molecular deposition. A surface-enhanced THz spectrum was clearly observed.

#249242 Received 1 Sep 2015; revised 17 Oct 2015; accepted 21 Oct 2015; published 23 Oct 2015

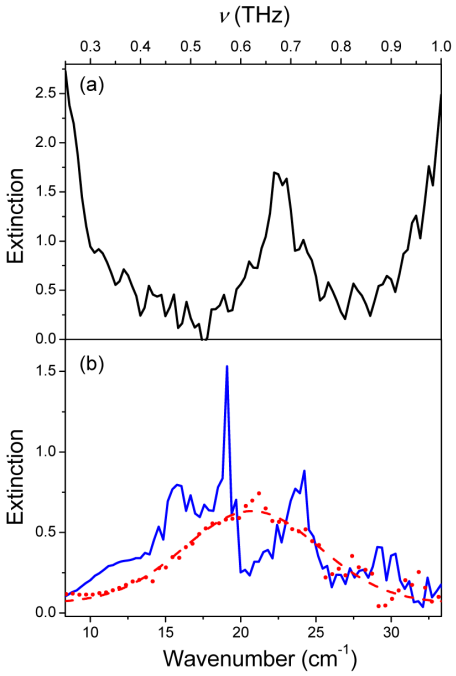

Fig. 3. (a) Extinction spectrum of the L-sodium glutamate pellet with a thickness of 0.9 mm. (b) Extinction spectra of the gold rod structured silicon substrate before the deposition of L-sodium glutamate (red) and after deposition of L-sodium glutamate (blue), respectively. The structure design was the same as the 100-μm-long gold rod structure presented in Fig. 1(b).

In the case of the molecular deposition method using drop casting and air-drying, it is difficult to control how many molecules are deposited on the structures and to make a uniform molecular film on the substrate. Because the deposition of L-glutamic acid on the silica-surfaced substrate by the evaporation method under low pressure conditions and its characteristics have been established [35], we deposited L-glutamic acid on the gold rod (length: 80 μm) structured silicon substrate using a vacuum evaporator (RD-1200, Sanvac Co.). During evaporation under low-vacuum conditions, the molten L-glutamic acid induces dehydration reactions, such as intramolecular cyclization forming L-pyroglutamic acid crystals and intermolecular dimerization or polymerization forming a poly-L-glutamic acid-film [35,36]. We deposited L-glutamic acid on the gold rod structures with a thickness of 150 nm. Figure 4(a) presents the FT-IR transmission spectra of the deposited poly-L-glutamic acid and L-pyroglutamic acid crystal on a silicon substrate. Although the structure was produced by chance, the spectra were successfully assigned based on literature values [35]. Figure 4(b) presents the surface-enhanced THz spectra of the corresponding deposited film. Similarly to the FT-IR spectrum, the relatively shaper peaks appeared when measuring the L-pyroglutamic acid crystal, and the relatively broad bands were observed when measuring the poly-L-glutamic acid film. Importantly, in the case of the L-pyroglutamic acid crystal, the LSPR band was split into two peaks at shorter and longer wavelengths compared with the original LSPR band. This splitting is similar to the spectrum of L-sodium glutamate crystal presented in Fig. 3(b).

On the other hand, Tominaga et al. reported a THz spectrum of L-poly-glutamic acid and found a broad spectrum with a steady increase from 6 to 30 cm^{-1} [37]. In their spectrum, small absorption bands at approximately 19, 22, 27, and 29 cm^{-1} were noted in the broad spectrum in the case of the random coil structure of the L-poly-glutamic acid [37]. It is possible that the small bands at approximately 18, 23 and 28 presented in Fig. 4(b) correspond with the reported absorption bands and have been enhanced according that the apparent absorption cross-section enhancement due to the increased dephasing time of LSPR.

#249242 Received 1 Sep 2015; revised 17 Oct 2015; accepted 21 Oct 2015; published 23 Oct 2015

However, the splitting of the spectrum was not observed in the case of the polymer. We hypothesize that dipole coupling, similarly to a strong coupling phenomenon, was exclusively induced in the crystal because the oscillator strength of the molecular/intermolecular vibrational mode of crystal is stronger than that of the polymer. The assignment of each band is important and necessary to understand the mechanism in further detail. However, the experiment suggests that it is possible to discern the molecular structure using the surface-enhanced THz spectroscopy if library data are obtained.

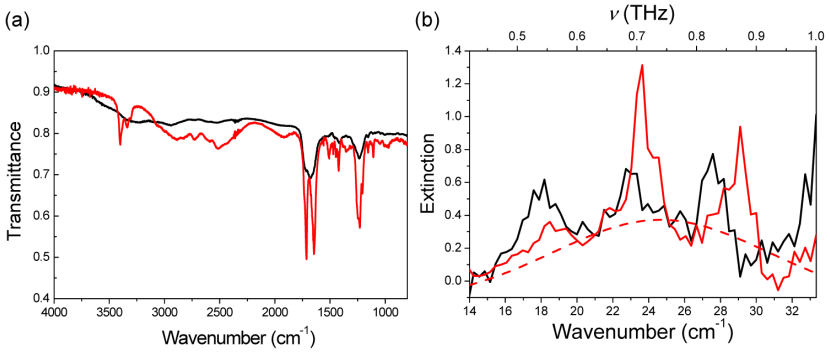

Fig. 4. (a) FT-IR transmission spectra of the L-glutamic acid film constituted from poly-L-glutamic acid (black) and L-pyroglutamic acid (red). (b) Surface-enhanced THz spectra of the L-glutamic acid film composed of poly-L-glutamic acid (black) and L-pyroglutamic acid (red). The broken red line indicates the traced LSPR band of the gold rod structure with a length of 80 μm before the deposition of L-glutamic acid.

Notably, the distinct surface-enhanced THz spectrum was successfully obtained even with a film only 50 nm thick as a separate experiment. Figure 5 depicts the extinction spectra of the L-glutamic acid film composed of L-pyroglutamic acid and D-pyroglutamic acid. Although there is a possibility that L-pyroglutamic acid film also contains a small amount of D-pyroglutamic acid due to racemization under the deposition process, the ratio of D-pyroglutamic acid was negligibly small [35]. As presented in Fig. 5, almost analogous spectra were obtained. This indicates that the spectrum of L- and D-pyroglutamic acid is almost same, and the reproducibility of the spectral measurement in the surface-enhanced THz spectroscopy is very high.

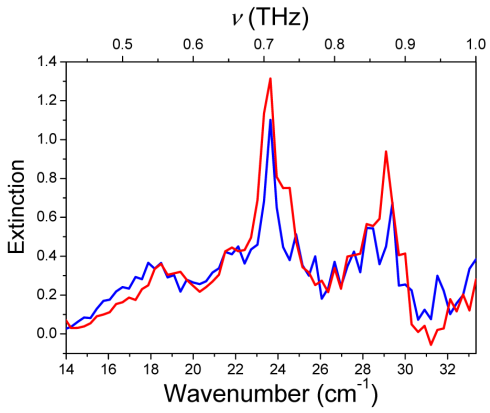

Fig. 5. Surface-enhanced THz spectra of L- and D-glutamic acid films composed of L-pyroglutamic acid (red) and D- pyroglutamic acid (blue). The spectrum of L-pyroglutamic acid was obtained from Fig. 4(b).

#249242 Received 1 Sep 2015; revised 17 Oct 2015; accepted 21 Oct 2015; published 23 Oct 2015

4. Conclusion

We successfully demonstrated surface-enhanced THz spectroscopy. The apparent absorption cross-section was enhanced due to the enhancement of a light-matter coupling process based on the longer dephasing time of LSPR in the THz frequency region, and the plasmon resonant spectrum was modulated by the change of the dielectric function by the coupling between the plasmon dipole and the dipole moment of the molecular/intermolecular vibrational modes. This interaction is very similar to that of a strong coupling between a microcavity and a molecular vibrational mode. Most importantly, the absorption spectrum of an amino acid-thin film was clearly observed due to LSPR excitation. However, it was difficult to observe such a spectrum without gold nanostructures in the frequency region from 0.3 to 1.0 THz. Because the frequency region experiences a relatively small influence from the absorption of water, applications of surface-enhanced THz spectroscopy are expected in the study of protein denaturation as well as structural changes of cell membranes.

Acknowledgments

We gratefully acknowledge financial support from MEXT-KAKENHI Photosynergetics (No. 15H01073), MEXT-KAKENHI AnApple (No. 15K00856), JSPS-KAKENHI (Nos. 23225006 and 15K04589), Nanotechnology Platform of MEXT (Hokkaido University), and Nano-Macro Materials, Devices and System Research Alliance of MEXT.

#249242 Received 1 Sep 2015; revised 17 Oct 2015; accepted 21 Oct 2015; published 23 Oct 2015